Continuum damage models with non-conventional finite element formulations

C.M. Silva, L.M.S.S. Castro

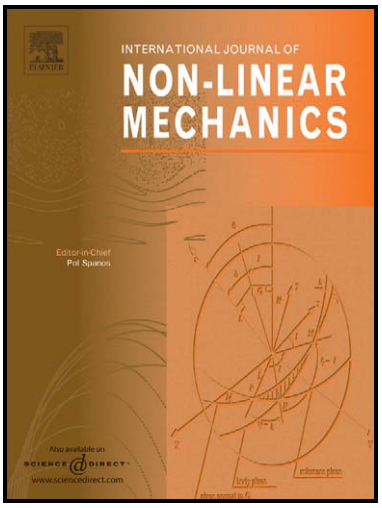

Continuum damage models with non-conventional finite element formulations

C.M. Silva, L.M.S.S. Castro

PII: S0020-7462(09)00170-X
DOI: doi:10.1016/j.ijnonlinmec.2009.09.005
Reference: NLM 1650

To appear in: *International Journal of Non-Linear Mechanics*

www.elsevier.com/locate/nlm

Received date: 12 March 2009
Revised date: 3 September 2009
Accepted date: 21 September 2009

Cite this article as: C.M. Silva and L.M.S.S. Castro, Continuum damage models with non-conventional finite element formulations, *International Journal of Non-Linear Mechanics*, doi:10.1016/j.ijnonlinmec.2009.09.005

Continuum damage models with non-conventional finite element formulations

C. M. Silva ** and L. M. S. S. Castro *

Departamento de Engenharia Civil e Arquitectura, Instituto Superior Técnico, Avenida Rovisco Pais, 1049-001 Lisbon, Portugal

Abstract

In recent years, some research effort has been devoted to the development of non-conventional finite element models for the analysis of concrete structures. These models use continuum damage mechanics to represent the physically non-linear behavior of this quasi-brittle material. Two alternative approaches proved to be robust and computationally competitive when compared with the classical displacement finite element implementations. The first corresponds to the hybrid-mixed stress model where both the effective stress and the the displacement fields are independently modeled in the domain of each finite element and the displacements are approximated along the static boundary, which is considered to include the inter-element edges. The second approach corresponds to a hybrid displacement model. In this case, the displacements in the domain of each element and the tractions along the kinematic boundary are independently approximated. Since it is a displacement model, the inter-element boundaries are now included in the kinematic boundary. In both models, complete sets of orthonormal Legendre polynomials are used to define all approximations required so very effective p-refinement procedures can be implemented. This paper illustrates the numerical performance of these two alternative approaches and compares their efficiency and accuracy with the classical finite element models. For this purpose, a set of numerical tests is presented and discussed.

Key words: hybrid and mixed finite element formulations, non-local damage models, Legendre polynomials

* email:luis@civil.ist.utl.pt,phone:+351+218418253
**email:cmsilva@civil.ist.utl.pt,phone:+351+218418356

Preprint submitted to Elsevier Science

1 Introduction

The main objective of the research work reported in this paper is the development of robust and computational competitive numerical techniques for the physically non-linear analysis of concrete structures.

The non-conventional hybrid and mixed finite element formulations used in this work were first developed by Freitas *et al* [16] during the nineties. Three main classes are defined, namely the hybrid-mixed, the hybrid and the hybrid-Trefftz formulations. Two models are derived for each formulation, the displacement and the stress models [45,5]. All formulations evolve directly from the first principles of mechanics, in particular equilibrium, compatibility and constitutive relations. What distinguishes the three types of formulations is the set of constraints enforced, *a priori*, on the domain approximations.

In recent years, some of these non-conventional finite element formulations have been extended to non-linear analysis using isotropic damage models [39–41,38,37].

In [39,34] the hybrid-mixed stress model based on the use of orthonormal Legendre polynomials [32] is chosen. The stress and the displacement fields in the domain of each element and the displacements on the static boundary are independently approximated. None of the fundamental relations is enforced a priori and all field equations are enforced in a weighted residual form, ensuring that the discrete numerical model embodies all the relevant properties of the continuum it represents. The Mazars' isotropic model [26] is adopted and a non-local integral formulation where the damage variable is taken as the non-local variable is considered.

In [35,40] an improved hybrid-mixed stress model is presented and discussed. The approximation of the stress field in the domain is here replaced by the approximation of the effective stress field. The isotropic damage models presented by Comi and Perego [11,9] are now adopted using a non-local integral model. An alternative technique based on the definition of an explicit enhanced gradient model has also been tested [38].

The use of hybrid-Trefftz displacement formulations, where the displacements in the domain of each element and the stress field on the kinematic boundary are independently approximated, is reported in [36,41]. The main feature of these models is that the functions used to approximate the displacements are derived from bi-harmonic displacement potentials that solve the Navier equations for a homogeneous elastic material [17,5]. Due to the strategy used in their definition, only while concrete presents a linear elastic behavior the model may be considered as a pure hybrid-Trefftz formulation. When this behavior is no longer valid, it becomes an hybrid-displacement model.

The use of hybrid-displacement models with Legendre polynomials is reported in [38,42]. An isotropic model with a non-local integral formulation is again adopted.

The main objective of this paper is to compare the numerical efficiency of the two most promising non-conventional finite element formulations implementing damage mechanics models, namely the hybrid-mixed stress model with the independent approximation of the effective stress field and the hybrid-displacement formulation with Legendre polynomials. A set of classical benchmark tests is chosen to illustrate the use of such models and to assess and compare their numerical performance. Comparisons are also made with solutions obtained with the classical finite element formulation, to prove that the proposed models are competitive.

The numerical models are both incremental and iterative and are solved with a modified Newton-Raphson method that uses the secant matrix. The models are implemented in a C program and all tests were run on a Pentium IV Machine, 2996 Mhz, running Linux.

This paper is organised as follows: the formulation of the problem and the adopted damage models are presented in Section 2 and 3. The non-conventional finite element formulations are described in Section 4. The numerical examples are shown in Section 5 and finally, Section 6 summarises the main conclusions and indicates future research work in this field.

2 Fundamental relations

Consider a domain V limited by the boundary Γ, referred to a cartesian coordinate system. The static boundary Γ_σ (or Neumann boundary) and the kinematic boundary Γ_u (or Dirichlet boundary) are complementary sub-regions of the boundary Γ, whereon traction-resultants and displacements are respectively prescribed.

The body under analysis is assumed to be homogeneous and isotropic. The model is geometrically linear and only static and monotonic loads are considered. No viscous, thermal or other non-mechanical dissipative effects are taken into account.

The fundamental equilibrium equations may be written in a matrix form as follows:

$$\begin{aligned} &\mathbf{D}\,\boldsymbol{\sigma} + \mathbf{b} = \mathbf{0} \quad \text{in} \quad V, \\ &\mathbf{N}\,\boldsymbol{\sigma} = \mathbf{t}_\gamma \quad \text{on} \quad \Gamma_\sigma, \end{aligned} \tag{1}$$

where $\mathbf{D}$ is the differential equilibrium operator. The matrix $\mathbf{N}$ contains the components of the unit outward normal vector to the static boundary Γ_σ. The vector $\boldsymbol{\sigma}$ lists the independent components of the stress tensor. The vector $\mathbf{b}$ represents the body force vector in the domain V and $\mathbf{t}_{\boldsymbol{\gamma}}$ corresponds to the tractions vector on the static boundary Γ_σ.

The compatibility equations may be written in the following format:

$$\begin{aligned} \boldsymbol{\varepsilon} &= \mathbf{D}^* \mathbf{u} \quad \text{in} \quad V, \\ \mathbf{u} &= \overline{\mathbf{u}} \quad \text{on} \quad \Gamma_u, \end{aligned} \tag{2}$$

where $\mathbf{D}^*$ is the differential compatibility operator, adjoint of the differential equilibrium operator $\mathbf{D}$ since the model is geometrically linear. The vector $\boldsymbol{\varepsilon}$ collects the independent components of the strain tensor and the vector $\mathbf{u}$ lists the independent components of the displacement field. The vector $\overline{\mathbf{u}}$ denotes the prescribed displacements on the boundary Γ_u.

The constitutive relation depends on the damage model adopted, as detailed in Section 3.

3 Non-local Damage Model

The mechanical behavior of quasi-brittle materials such as concrete, is characterised by the development of micro-cracks and subsequent evolution to localised macro cracking. The Continuum Damage Mechanics models describe the evolution of the mechanical properties of the continuum as cracking develops. This type of constitutive models are able to describe, with a continuum approach, some of the material properties observed in experiments, such as global softening, stiffness degradation, anisotropy and development of inelastic deformations [43,27,23,18,10].

In this paper, two different damage models are considered. The first one (Model 1) corresponds to a simple isotropic continuum damage model with only one damage variable used e.g. in the works of [25,11,12]. The second model (Model 2) considers two independent damage variables and was introduced by Comi and Perego in [9,10,7]. In both models, plastic strains are neglected. The two adopted models are presented summarily in Tables 1 and 2.

The strain softening behavior is well known to produce strain localization with consequent dependence on the data of the finite element model, as for instance the dependence on the mesh and on the degrees of the approximation functions [1,21]. To overcome this problem, several regularisation techniques are proposed in the literature, in particular non-local integral [33,2] and gradient-enhanced damage formulations [29,6]. Following Pijaudier-Cabot and Bažant

[33], the present work assumes a non-local integral analysis for both damage models. When the model with one damage variable is used, the strain energy release rate is adopted as the non-local variable. When using the second model, the strain invariants involved in the definition of the constitutive laws are defined as non-local variables.

As defined in [33], a generic non-local variable $\overline{v}$ is computed considering the following weighted average over the whole domain:

$$\overline{v}(x) = \int_V W(x,s)\; v(s)\, \mathrm{d}s \;,$$

where $W(x,s)$ is a weight function taken here as the normalised Gauss function:

$$W(x,s) = \frac{1}{W_0(x)} \exp\left(-\frac{\|x-s\|^2}{2\,l^2}\right),\; W_0(x) = \int_V \exp\left(-\frac{\|x-s\|^2}{2\,l^2}\right) \mathrm{d}s \;.$$

The length l in the previous equation is a geometric length, usually denoted as *characteristic length*. It works as a localisation limiter and regularises the mathematical problem. According to [3], this length may also be interpreted as a material-dependent parameter related to the width of the fracture process zone. A normalised weight function is chosen because the non-local model should be able to reproduce correctly local uniform fields.

Model 1 has the limitation of considering the same behavior for the material in prevailing tension and compression states, which is not realistic for most of the materials. To overcome this limitation, it is assumed that damage may only appear and develop if the strain tensor trace is positive, $tr\,\boldsymbol{\varepsilon} > 0$. The constitutive model with the referred assumption is suitable for studying structures subjected mainly to tension stresses and it is competitive due to its simplicity.

Model 2 requires more computational effort than Model 1. This happens because it is not possible to define explicitly the values of d_t and d_c in terms of the potentials f_t and f_c. On the other hand, the non-local integral model to be used [7] is more demanding from the computational point of view.

4 Non-conventional Finite Element Formulations

4.1 Hybrid-mixed Stress Formulation (HMS)

The hybrid-mixed stress formulation adopted in this work was for the first time described in [40]. Compared to the original version of the hybrid-mixed stress formulation [16] the particularity of the new model is that the approximation of the stress field $\boldsymbol{\sigma}$ is replaced by the approximation of the effective stress field $\widetilde{\boldsymbol{\sigma}}$, defined e.g. by Lemaitre in [25]. The approximations may be expressed as:

$$\begin{aligned} \widetilde{\boldsymbol{\sigma}} &= \mathbf{S}_v \, \widetilde{\mathbf{X}} \ \text{ in } \ V, \\ \mathbf{u} &= \mathbf{U}_v \, \mathbf{q}_v \ \text{ in } \ V, \\ \mathbf{u} &= \mathbf{U}_\gamma \, \mathbf{q}_\gamma \ \text{ on } \ \Gamma_\sigma, \end{aligned} \tag{3}$$

where the matrices $\mathbf{S}_v$, $\mathbf{U}_v$ and $\mathbf{U}_\gamma$ collect the approximation functions and the vectors $\widetilde{\mathbf{X}}$, $\mathbf{q}_v$ and $\mathbf{q}_\gamma$ list the associated weights (generalised variables). Since the three fields are approximated independently, it is possible to adopt different degrees of approximation for each one.

Due to the properties presented by Legendre polynomials, it is possible to increase the degree of the approximations without having any problems in terms of numerical stability. This fact enables the implementation of highly efficient p-refinement procedures, as it is possible to define high degree approximations without deteriorating the condition number of the global governing system. In order to ensure the numerical stability of the hybrid-mixed stress model, it is necessary to ensure that the number of stress parameters (number of degrees of freedom associated with the approximation of the static fields) is greater than the number of displacement parameters (number of degrees of freedom associated with the approximation of the kinematic fields). To avoid spurious kinematic modes, it is also important to ensure that the degrees of the Legendre polynomials used in the displacement fields approximation is smaller than the polynomial degrees involved in the effective stress components approximation [16].

While the concrete is linear elastic, the model proposed coincides with the one described in [16]. When damage appears, the models are different since the effective stress and the stress field are no longer coincident. In the context of a non-linear analysis with softening, the main advantage of the proposed approach when compared to the one described by Freitas [16] is that the effective stress field is directly related to the evolution of damage, since it is comparable to the to the strain field, while the stress field is not.

The generalised strains, $\mathbf{e}$, body forces, $\mathbf{Q}_v$, and tractions, $\mathbf{Q}_\gamma$ are defined by

$$\mathbf{e} \;=\; \int \mathbf{S}_v^t\, \boldsymbol{\epsilon}\, \mathrm{d}V, \qquad \mathbf{Q}_v \;=\; \int \mathbf{U}_v^t\, \mathbf{b}\, \mathrm{d}V, \qquad \mathbf{Q}_\gamma \;=\; \int \mathbf{U}_\gamma^t\, \mathbf{t}_\gamma\, \mathrm{d}\Gamma_\sigma, \tag{4}$$

in order to ensure the inner product invariance between the pairs of dual discrete variables $(\widetilde{\mathbf{X}}\,,\, \mathbf{e})$, $(\mathbf{q}_v\,,\, \mathbf{Q}_v)$, and $(\mathbf{q}_\gamma\,,\, \mathbf{Q}_\gamma)$ and the continuum fields they represent.

As demonstrated in [35,40,38], using the definition of the effective stress in the form $\boldsymbol{\sigma} = \widetilde{\boldsymbol{\sigma}}\,(1-d)$ [25] and enforcing the fundamental equations (Section 2) on average, in the sense of Galerkin, one obtains the following equilibrium equations for the discrete model:

$$\begin{aligned} (\mathbf{A}_v^t - \mathbf{M}_v)\,\widetilde{\mathbf{X}} &= -\mathbf{Q}_v \qquad \text{in } V, \\ (\mathbf{A}_\gamma^t - \mathbf{M}_\gamma)\,\widetilde{\mathbf{X}} &= \mathbf{Q}_\gamma \qquad \text{on } \Gamma_\sigma, \end{aligned} \tag{5}$$

where the matrices $\mathbf{M}_v$, $\mathbf{M}_\gamma$ and $\mathbf{A}_v$, $\mathbf{A}_\gamma$ are defined as follows:

$$\begin{gathered} \mathbf{M}_v = -\int (\mathbf{D}^*\mathbf{U}_v)^t\, \mathbf{S}_v\, d\, \mathrm{d}V + \int (\mathbf{N}^*\mathbf{U}_v)^t\, \mathbf{S}_v\, d\, \mathrm{d}\Gamma, \quad \mathbf{M}_\gamma = \int \mathbf{U}_\gamma^t\, (\mathbf{N}\mathbf{S}_v)\, d\, \mathrm{d}\Gamma_\sigma, \\ \mathbf{A}_v = \int (\mathbf{D}\mathbf{S}_v)^t\, \mathbf{U}_v\, \mathrm{d}V, \quad \mathbf{A}_\gamma = \int (\mathbf{N}\mathbf{S}_v)^t\, \mathbf{U}_\gamma\, \mathrm{d}\Gamma_\sigma. \end{gathered} \tag{6}$$

In a more complex damage model, as the Model 2 described in Section 3, a similar procedure may be followed to define matrices $\mathbf{M}_v$ and $\mathbf{M}_\gamma$ [38].

The compatibility condition in the discrete model (Equation (7)) may be obtained integrating by parts the average enforcement of the compatibility equation in the domain and then replacing in the resulting expression the approximations for the displacements (Equation (3)) [35,40]:

$$\mathbf{e} = -\mathbf{A}_v\, \mathbf{q}_v + \mathbf{A}_\gamma\, \mathbf{q}_\gamma + \overline{\mathbf{e}}, \qquad \text{with} \qquad \overline{\mathbf{e}} = \int (\mathbf{N}\mathbf{S}_v)^t\, \overline{\mathbf{u}}\, \mathrm{d}\Gamma_u. \tag{7}$$

The relation between the independent components of the effective stress tensor and the strain components can be expressed as [40]:

$$\boldsymbol{\epsilon} = \mathbf{F}\, \widetilde{\boldsymbol{\sigma}}\,, \tag{8}$$

where $\mathbf{F}$ is the symmetric non-singular matrix of elastic constants characterizing a linear reciprocal elastic law.

Introducing the constitutive relation (Section 3) and the generalised strains (Equation (4)) in Equation (7), we obtain Equation (9) that englobes the

compatibility and the constitutive relations of the discrete model:

$$\mathbb{F}\,\widetilde{\mathbf{X}} + \mathbf{A}_v\,\mathbf{q}_v - \mathbf{A}_\gamma\,\mathbf{q}_\gamma = \overline{\mathbf{e}}, \qquad \text{with} \qquad \mathbb{F} = \int \mathbf{S}_v^t\,\mathbf{F}\,\mathbf{S}_v\,\mathrm{d}V. \tag{9}$$

Combining Equation (5) and (9), one obtains the following solving system for each finite element:

$$\begin{bmatrix} \mathbb{F} & \mathbf{A}_v & -\mathbf{A}_\gamma \\ (\mathbf{A}_v^t - \mathbf{M}_v) & \mathbf{0} & \mathbf{0} \\ -(\mathbf{A}_\gamma^t - \mathbf{M}_\gamma) & \mathbf{0} & \mathbf{0} \end{bmatrix} \begin{Bmatrix} \widetilde{\mathbf{X}} \\ \mathbf{q}_v \\ \mathbf{q}_\gamma \end{Bmatrix} = \begin{Bmatrix} \overline{\mathbf{e}} \\ -\mathbf{Q}_v \\ -\mathbf{Q}_\gamma \end{Bmatrix}. \tag{10}$$

The governing system of the finite element mesh is assembled by direct allocation of the contribution of the elementary systems [16].

According to Equation (10), when a damage mechanism in a finite element is active, the elementary governing system is nonsymmetric, since $\mathbf{M}_v \neq \mathbf{0}$ and $\mathbf{M}_\gamma \neq \mathbf{0}$. Nevertheless, the governing system remains very sparse and the non-local behavior due to damage appears in the "small dimension" of the system (Figure 1).

Because the non-conventional models adopted in this work use macro-element meshes, it is not possible to control the length of the nonlinear strain localization band through the finite element mesh, as usually happens in a traditional displacement formulation. Consequently, a more refined mesh must be chosen to implement the nonlocal integral model. In this work, the Lobatto points mesh is used for this purpose. Another choice would also be valid. The choice of the Lobatto points mesh is adopted because this mesh is already defined to ensure the accuracy of the numerical integrations. Since the hybrid-mixed stress model requires the knowledge of the damage evolution on the boundary, the Lobatto quadrature rule is used instead of the usual Gauss quadrature rule. In order to capture the strain localization band, it is necessary to ensure that a convenient number of Lobatto control points lie inside the process zone, so the number of control points must be large (at least 10×10 per element), as shown in the numerical tests presented in the paper.

The algorithm used in the solution of the non-linear governing system follows a secant Newton-Raphson method. At load step j the iterative algorithm can be described by the following steps:

(1) Initialize the variables by setting $\mathbf{v}_0 = \mathbf{v}^{(j-1)}$
(2) Error= $10\times$ *tol* and *iter*=1
(3) *while* Error $>$ *tol*

(a) $iter$=$iter$+1
(b) computation of the non-local variable at each Lobatto point;
(c) validation of the Kuhn-Tucker conditions (see Tables 1 and 2) in order to define the new values for the damage variable;
(d) computation of the secant matrix, $\mathbf{A}$;
(e) computation of the residual vector, $\mathbf{R}$;
(f) solution of the system $\mathbf{A}\,\boldsymbol{\Delta}\mathbf{s}ol = -\mathbf{R}$;
(g) update the value for the generalized variables, $\mathbf{s}ol_{iter} = \mathbf{s}ol_{iter-1} + \boldsymbol{\Delta}sol$;
(h) computation of the new value for the controlling parameter, Error;

(4) store the final value for the generalized variables, $\mathbf{v}^{(j)} = \mathbf{v}_{iter}$.

In the hybrid-mixed stress model, the secant operator $\mathbf{A}$ corresponds to the matrix presented in Eq.(10). The solution vector $\mathbf{v}$ collects the generalized effective stress parameters, $\widetilde{\mathbf{X}}$, and the generalized domain and static boundary displacement variables, $\mathbf{q}_v$ and $\mathbf{q}_\gamma$. The residual vector $\mathbf{R}$ is defined according to Eq.(10).

4.2 Hybrid Displacement Formulation (HD)

Let us express the approximations as:

$$\begin{aligned} \mathbf{u} &= \mathbf{U}_v\,\mathbf{q} \qquad \text{in } \mathrm{V}, \\ \mathbf{t} &= \mathbf{T}\;\mathbf{p} \qquad \text{on } \Gamma_\mathrm{u}, \end{aligned} \tag{11}$$

where the matrices $\mathbf{U}_v$ and $\mathbf{T}$ collect the approximation functions for the displacements in the domain and for the tractions on the boundary Γ_u. The vectors $\mathbf{q}$ and $\mathbf{p}$ list the associated weights. As each field is approximated independently, the approximations may be refined separately.

Enforcing the inner product invariance between discrete and continuum dual quantities, it is possible to obtain the following generalised displacements $\mathbf{v}$ and the generalised body forces $\mathbf{Q}_v$:

$$\mathbf{v} \;=\; \int \mathbf{T}^t\;\overline{\mathbf{u}}\;\mathrm{d}\Gamma_u, \qquad \mathbf{Q}_v \;=\; \int \mathbf{U}_v^t\;\mathbf{b}\;\mathrm{d}V. \tag{12}$$

In the hybrid displacement formulation, the equilibrium in the domain and the continuity between elements is enforced on average, in a weighted-residual form, using the compatibility equation on Γ_u. It can be shown [41] that the first set of equations in the discrete model is:

$$\widetilde{\mathbb{K}}\,\mathbf{q} - \mathbf{B}\,\mathbf{p} = \mathbf{Q}_v + \mathbf{Q}_\Gamma \qquad \text{in } V, \tag{13}$$

where:

$$\begin{aligned} \widetilde{\mathbb{K}} &= \int (\mathbf{D}^*\,\mathbf{U}_v)^t\ \widetilde{\mathbf{K}}\ (\mathbf{D}^*\,\mathbf{U}_v)\ \mathrm{d}V, \\ &\text{with}\quad \widetilde{\mathbf{K}} = \mathbf{K}\,(1-d), \\ \mathbf{B} &= \int \mathbf{U}_v^t\ \mathbf{T}\ \mathrm{d}\Gamma_u, \\ \mathbf{Q}_\Gamma &= \int \mathbf{U}_v^t\ \mathbf{t}_\gamma\ \mathrm{d}\Gamma_\sigma, \end{aligned} \tag{14}$$

In the discrete model, the compatibility equation on the boundary Γ_u is given by [41]:

$$-\mathbf{B}^t\,\mathbf{q} = -\mathbf{v} \quad \text{on } \Gamma_u. \tag{15}$$

The combination of Equation (13) and (15) leads to the following solving system for each finite element:

$$\begin{bmatrix} \widetilde{\mathbb{K}} & -\mathbf{B} \\ -\mathbf{B}^t & \mathbf{0} \end{bmatrix} \begin{Bmatrix} \mathbf{q} \\ \mathbf{p} \end{Bmatrix} = \begin{Bmatrix} \mathbf{Q}_v + \mathbf{Q}_\Gamma \\ -\mathbf{v} \end{Bmatrix}. \tag{16}$$

Again, the governing system of the finite element mesh is assembled by direct allocation of the contribution of each elementary system [16].

Because the material is assumed to be non-linear, all the coefficients of the elementary generalised stiffness matrix $\widetilde{\mathbb{K}}$ are *a priori* nonzero, see Figure 2(b). Since the dimension of the matrix $\widetilde{\mathbb{K}}$ is the most important dimension of the governing system, it can become computationally very expensive to store and to solve the non-linear system in the form (16). In order to optimize the numerical performance of the hybrid displacement formulation, two different implementations are considered:

- Implementation 1 (I1): to solve the governing system in the form (16);
- Implementation 2 (I2): to update the generalised stiffness matrix $\widetilde{\mathbf{K}}$ in load step n whenever the number of iterations in load step $(n-1)$ is higher than a certain fixed value. An additional vector on the right hand side of the governing system is introduced, $\boldsymbol{\sigma}_0$:

$$\boldsymbol{\sigma} = \widetilde{\mathbf{K}}\,\boldsymbol{\varepsilon} = \mathbf{K}\,(1-d_0)\,\boldsymbol{\varepsilon} + \boldsymbol{\sigma}_0, \tag{17}$$

where d_0 corresponds to the damage distribution when the operator $\widetilde{\mathbf{K}}$ was last updated. It is possible to write:

$$\boldsymbol{\sigma} = \widetilde{\mathbf{K}}\,\boldsymbol{\varepsilon} = \mathbf{K}\,(1-d)\,\boldsymbol{\varepsilon} = \mathbf{K}\,(1-d_0+d_0-d)\,\boldsymbol{\varepsilon},$$

yielding the following definition for vector $\boldsymbol{\sigma}_0$

$$\boldsymbol{\sigma}_0 = \mathbf{K}\,(d_0-d)\,\boldsymbol{\varepsilon},$$

The equilibrium equation is in this case given by:

$$\widetilde{\mathbb{K}}_n^0\,\mathbf{q} - \mathbf{B}\,\mathbf{p} = \mathbf{Q}_v + \mathbf{Q}_\Gamma + \overline{\mathbf{Q}}_* \qquad \text{in } V, \tag{18}$$

with:

$$\widetilde{\mathbb{K}}_n^0 = \int (\mathbf{D}^*\,\mathbf{U}_v)^t\;\mathbf{K}\,(1-d_0)\;(\mathbf{D}^*\,\mathbf{U}_v)\;\mathrm{d}V;\;\overline{\mathbf{Q}}_* = \int (\mathbf{D}^*\,\mathbf{U}_v)^t\;\mathbf{K}\;\boldsymbol{\varepsilon}\,(d-d_0)\;\mathrm{d}V. \tag{19}$$

Once more, the expressions presented in this paper assume an isotropic model with only one damage variable. If this is not the case, the final expressions are somewhat different and may be found in [38]. However, all conclusions illustrated are still valid.

For the solution of the non-linear governing system it is adopted an algorithm similar to the one presented for the hybrid-mixed stress model.

5 Numerical Applications

Three tests are presented: the Hassanzadeh's test, an L-shaped plate and a gravity dam.

The Hassanzadeh's test is used here to compare the performance of the hybrid-mixed stress model (HMS), the hybrid displacement (HD) model and the classical displacement finite element formulation (FEM).

Initially, the numerical performance of the HMS model is evaluated and compared with the classical FEM, using the numerical results obtained by Claudia Comi, partly published in [7]. In this analysis, the two damage variable model described in Section 3 is chosen. The global load-displacement diagrams and the damage and strain distributions obtained with both models are directly compared. The relative numerical efficiency is qualitatively evaluated using for this purpose the number of iterations required in each step of the loading procedure. It is not useful to compare directly the CPU time since the tests were run using different hardware.

Then, the numerical performance of the HMS and HD models is assessed assuming a simpler damage model (Model 1 presented in Section 3). The strain field distributions, the CPU time required to complete the analysis and the number of iterations in each step of the loading procedure are compared.

5.1 Hassanzadeh's test [19]

The Hassanzadeh's test is illustrated in Figure 3(a). Due to the geometry and to the applied load, only the tension mechanism is activated through the loading history. The structure is analysed as a strain plane problem. In all discretizations a (20×20) Lobatto mesh points is used in each element.

5.1.1 HMS versus FEM

The two variable damage model described in Section 3 is used. Following [7] the material parameters are: $a_t = 0.31$, $b_t = 4.4$ MPa, $k_t = 15.1$ MPa^2, $c_t = 35$, $d_{ot} = 0.10$, $(\sigma_e/\sigma_o)_t = 0.80$, $l_t = 1.0$ mm, $E = 36000$ MPa and $\upsilon = 0.15$.

Table 3 lists the main characteristics of the discretizations associated with each one of the models. The Legendre polynomial degrees adopted to define the approximation for both the stress ($\mathbf{S}_v$) and the displacement ($\mathbf{U}_v$) fields in the domain are given in columns 2 and 3, for the case of Test I and Test II, respectively. The same table lists also the polynomial degrees involved in the definition of the displacement field along the static boundary ($\mathbf{U}_\gamma$).

In all discretizations, the approximation is refined near the center of the structure, because the higher stress gradients are located exactly in that region. The FEM meshes use constant strain triangle (CST) elements and correspond to the meshes adopted by Claudia Comi in [7], see Figure 4. For the HMS model two different discretizations are adopted, both using a 7 element mesh (Figure 3(b)), but considering different approximation degrees. Test I refines the approximation mainly at the vertical direction, where Test II uses the same degree of approximation in both directions.

Figure 5 presents the reaction R - prescribed displacement $\overline{u}$ diagrams, obtained with the numerical simulations and with the experimental test. Both numerical formulations, the HMS and the FEM, correctly model the experimental behavior, except for the experimental bump. On the other hand, the results provided by the different numerical models are almost coincident.

Figure 6 shows that also the damage distribution evolution obtained with both

numerical models is quite similar.

As shown in Table 3, the use of HMS models leads to larger number of degrees of freedom, N_{dof}. However, the iterative procedure associated with the proposed HMS formulation is less demanding. Figure 7 shows the evolution of the number of iterations required by each incremental load step in terms of the prescribed displacement $\overline{u}$. This information is plotted for the HMS Tests I and II and for the FEM hd00d Test. Both formulations use constant local increments and a secant Newton-Raphson technique for the solution of the non-linear governing system. Test hd00d requires 800 load steps until the final prescribed value, $\overline{u} = 0.040$ mm, is reached. The test cases run with the HMS model use either 40 or 200 load steps, as indicated in Figure 7. For both formulations it is possible to notice an increase in the number of iterations near the maximum load peak and when the stress dissipation starts to greatly influence the behavior of the structure. In spite of using a larger number of load steps, the curve associated with Test hd00d is always above the curves obtained with the HMS models. When comparing the two tests involving this later model, it is possible to notice a significant decrease in the number of iterations when using 200 load steps instead of 40. This decrease would be even greater if 800 load steps would have been used. This qualitative study indicates that the HMS model is more stable from the numerical point of view than the classical displacement finite element formulations, requiring less number of iterations in each load step to converge [1] .

The numerical stability associated with the use of HMS models can be explained by the accuracy of the numerical solution obtained for the strain field, $\boldsymbol{\varepsilon}$, which is used to define and control the material damage evolution and the corresponding mechanical structural behavior. On one hand, in the HMS formulation, the strain field $\boldsymbol{\varepsilon}$ is directly computed using the approximation defined for the effective stress fields, $\widetilde{\boldsymbol{\sigma}}$. When using the classical finite element formulation, the computation of the strain field $\boldsymbol{\varepsilon}$ requires the definition of displacement field derivatives. On the other hand, since the damage distribution is continuous, the inter-element continuity of the fields $\widetilde{\boldsymbol{\sigma}}/\boldsymbol{\varepsilon}$ is enforced in a weighted residual form in the HMS model through the equilibrium equation on the static boundary. On the contrary, the FEM formulation using the same non-local damage model does not satisfy the inter-element strain continuity. Moreover, the HMS formulation works with macroelements and adopts preferentially a p-refinement instead of an h-refinement, minimizing the number of inter-element boundaries.

[1] Please note that the error criteria is probably not the same for both formulations, so the comparison made in this paper is only qualitative. However, it is shown that the three tests lead to identical results in terms of global behavior and damage distribution, so the qualitative comparison is adequate.

The accuracy of the strain field in each formulation may be confirmed by the analysis of Figures 8 and 9, where the evolution of the vertical strain field, ε_{yy} for Tests I and hd00d is shown. This strain component is chosen since it is the one that most influences the non-linear behavior of the structure. The ε_{yy} distribution is quite different in both formulations. The HMS solution shows a smooth variation of this physical quantity in the vertical direction, while the strain field ε_{yy} obtained with the FEM formulation is clearly discontinuous between elements.

5.1.2 HMS versus HD

In this comparative analysis, the model with one damage variable, presented in Section 3, is considered. The corresponding material parameters are given by $n = 12, k = 5.8 \times 10^{-14}$ MPa, $c = 405, l = 1.6$ mm, $E = 36$ GPa and $\nu = 0.15$. These are the values used by Comi and Perego in [12]. All discretizations use the seven element mesh presented in Figure 3(b). The approximation details of each discretization are summarised in Table 4.

According to Figure 10, both models correctly model the global load-displacement diagram. Since the one variable damage model is associated with a larger characteristic length than the model with two damage surfaces [14,12], the global behavior in this case is not so brittle (Figure 7 versus Figure 10).

According to the values presented in Table 4, although the HMS models are associated with a larger number of degrees of freedom when compared to the HD models, the CPU time required by the HMS implementations is always smaller, specially if Implementation I1 (Section 4) is used with the HD formulation. The same happens even if the Implementation I2 (Section 4) is used. This behavior may be justified because the strain filed used in the definition of the damage evolution is obtained more precisely in the HMS model. In this model, the strain field is computed directly from the effective stress field approximation while in the HD formulation the strain field is obtained through the differentiation of the displacement fields modeled in the domain of each element. In terms of vertical strain distribution the final results are quite similar, as illustrated in Figure 11, where the ε_{yy} distribution is presented for all test cases. Only Test C presents a different behavior. However this difference can be overcome by increasing the degree of the approximation in the horizontal direction.

Figure 12 compares the number of iterations required by the convergence of each load step increment, assuming in all test cases a total number of 40 uniform load steps until a maximum prescribed displacement of $\overline{u} = 0.040$ mm is reached. When using an implementation I1, the number of iterations per

load step is similar when using the HMS or the HD models, see Tests A and B versus Test C (I1). As expected, a larger number of iterations is required near the peak of the load-displacement diagram. After that, the number of iterations required by each load increment decreases with the increase of the prescribed displacement. When compared to the case where the bi-dissipative damage model is used, the unloading process is smoother and there is no increase in terms of number of required iterations at the unloading region (Figure 7 versus Figure 12). As CPU times associated with Implementation I1 are unacceptable (see Table 4) the use of the Implementation I2 is highly recommended. In this case, the curve number of iterations versus prescribed displacement presents a very different behavior because the global governing system is updated only when the number of iterations required at the previous load step is greater than a given tolerance.

Since the results of Tests A and B are equivalent in terms of global response, strain field distribution and iterative procedure, one may conclude that the discretization of Test A is sufficiently accurate and that excessive p-refinement associated with a huge number of degrees of freedom (as in Test B) is not needed.

5.2 L-shaped plate

Let us consider the L-shaped concrete plate presented in Figure 13. The thickness of the plate is $100mm$ and an upward vertical displacement, $\overline{u}$, at the lowest right corner is prescribed.

The experimental results and the solutions obtained with several numerical simulations are available at the NWD-IALAD website [2] .

The numerical analysis presented here is based on the HMS model. The damage model with one damage variable presented in Section 4 is adopted in this case. The available experimental data are the Young modulus $E = 25850$ MPa, the Poisson coefficient, $\nu = 0.18$ and the maximum strength in tension, $f_t = 2.70MPa$. The remaining material parameters are defined in order to minimize the differences between the experimental and numerical load-prescribed displacement diagrams. The following values have been assumed: $n = 9.5, k = 1.1 \times 10^{-11}$ MPa, $c = 270$ and $l = 11$ mm.

A plane stress behavior is considered and the vertical displacement at the lower right corner is prescribed. Two different numerical tests have been performed. Test 1 considers the three element mesh represented in Figure 14. The discretization associated with this test uses $\mathbf{S}_v^{\xi,\eta} = 10$, $\mathbf{U}_v^{\xi,\eta} = 9$ and

[2] Currently, http://nw-ialad.uibk.ac.at/, grupo WP2/TG2, Test n. 1

$\mathbf{U}_{\gamma}^{\xi,\eta} = 7$, yielding a total of 1385 degrees of freedom. In each finite element, a (20×20) Lobatto mesh points is used to perform all numerical integrations and to compute the non-local variables. Test 2 uses the 10 element mesh shown in Figure 14 and assumes $\mathbf{S}_{v}^{\xi,\eta} = 7$, $\mathbf{U}_{v}^{\xi,\eta} = 6$ and $\mathbf{U}_{\gamma}^{\xi,\eta} = 6$. This discretization involves a total of 3251 degrees of freedom. In this case a (10×10) Lobatto mesh points is used.

The reaction-prescribed displacement $\overline{u}$ diagrams are presented in Figure 15. It is possible to confirm that both numerical and experimental diagrams are quite similar.

The evolution for the horizontal displacement at the upper left corner of the structure is shown in Figure 16. The numerical response is stiffer than the experimental behavior at the beginning of the loading procedure. This type of behavior is also observed in other numerical simulations and can be justified by the fact that the numerical simulation does not take into account the rotational stiffness of the steel device that embraces the L-shaped concrete structure.

Figure 17 presents the damage evolution and identifies the principal directions of the effective stress tensor. As expected, damage first appears near the reentrant corner with a diagonal orientation and evolves towards an almost horizontal macro crack.

Finally, Figure 18 shows the damage evolution represented in a deformed configuration. The damage appearing in the lower right corner is a local effect induced by the prescribed displacement imposition and does not interfere with the global behavior of the structure.

5.3 Koyna dam

The Koyna dam is located in the southern part of India. The geometry of this concrete gravity dam is presented in Figure 19(a). In December 1967, this dam was subjected to an important earthquake. In the last few years, several authors have tried to compute numerically the damage distribution installed due to that earthquake, see for instance [4,24].

The numerical study presented in this paper aims to identify the highest water lever in the reservoir ensuring dam security conditions considering an initial damage distribution caused directly by the earthquake, the dam self weight and the hydrostatic lateral pressure.

Following the work of [4], an initial qualitative damage distribution is taken into account, as illustrated in Figure 20. The initial damage distribution is con-

centrated near the structure-foundation interface and near the dam geometric change. Three different damage values are considered in the region with initial diffuse cracking (red region in Figure 20): $d_{\text{initial}} = 0.00$ (Test 1), $d_{\text{initial}} = 0.30$ (Test 2) and $d_{\text{initial}} = 0.60$ (Test 3). For the numerical simulations the HMS model is used.

A plane strain behavior is assumed. The finite element mesh presented in Figure 19(b) is used in the analysis. Following [20], the rock foundation is included in the finite element analysis. The degrees of approximation are defined by $\mathbf{S}_v^{\xi,\eta} = 5$, $\mathbf{U}_v^{\xi,\eta} = 4$, $\mathbf{U}_\gamma^{\xi,\eta} = 3$ and a (20×20) Lobatto mesh points is defined in each element.

The bi-dissipative damage model presented in Section 4 is used in the analysis. The material parameters for concrete and rock are defined according to [4,9]:

- for concrete: $E = 30$ GPa, $\upsilon = 0.20$, $\rho = 2630$ kg/m^3, $a_t = 0.25$, $b_t = 4.4$ MPa, $k_t = 9.14$ MPa^2, $c_t = 3.3$, $(\sigma_e/\sigma_o)_t = 0.70$ and $d_{ot} = 0.0$;
- for rock: $E = 41$ GPa, $\upsilon = 0.10$, $\rho = 2700$ kg/m^3, $a_t = 0.333$, $b_t = 3.3$ MPa, $k_t = 8.6$ MPa^2, $c_t = 3.3$, $(\sigma_e/\sigma_o)_t = 0.70$ and $d_{ot} = 0.0$.

The characteristic length is $l_t = 400$ mm. The behavior to compression states is considered to be linear elastic.

Figure 21 shows the evolution of the horizontal displacement measured at the top of the dam in terms of parameter $q = h_{\text{water}}/h_{\text{dam}}$. When evaluating the load carrying capacity and the safety of a dam against failure, it is a common procedure to consider values greater than unity for parameter q, leading to the so called *imminent failure flood* analysis.

The damage distribution is presented in Figure 22 for all three cases. It is possible to notice a significant damage evolution near the interface foundation-structure. There is also a slight damage increase at the region where de the geometry of the structure changes.

Interestingly, the comparison of the solutions obtained for the three cases shows that the initial damage value has a very little influence in terms of final collapse load and displacements fields. This conclusion was also obtained by other authors [4,9].

6 Conclusions

Two promising non-conventional finite element formulations, namely the hybrid-mixed stress (HMS) and the hybrid displacement (HD) models, are discussed in this paper. The main properties of such models and their numerical per-

formance are illustrated through the analysis of a set of classical benchmark tests.

The main conclusions can be summarised as follows:

(1) both the HMS and the HD models lead to stable and robust numerical procedures. The HMS models show better convergence rates than the classical displacement FEM implementations. This efficiency can be justified by the accuracy ensured for the effective stress/strain distributions that control the damage evolution behavior;
(2) in all performed numerical tests, the quality of the solutions does not depend on the finite element mesh orientation (*mesh bias*). This behavior results mainly from the use of macroelement meshes associated with the implementation of highly effective p-refinement procedures. As discussed in [22], this type of phenomena may influence the quality of the results provided by the classical FEM computations;
(3) the HMS model may lead to *quasi*-equilibrated solutions. Consequently, this model may provide lower bounds for the structure collapse loads.

The physically non-linear analysis of concrete structures is still a challenge and corresponds to an application field where the high performance alternative formulations presented in this paper can be conveniently explored.

The fracture processes strongly influence the structural behavior of concrete structures and may be modeled using continuous or discrete approaches. One strong drawback associated to the application of pure continuous models lies in the fact that fragile rupture is frequently governed by the growth of a dominant crack. Although both approaches continue to deserve the scientific community attention, the current trend is clearly to combine the two methodologies. Therefore, the main expected development corresponds to the implementation of cohesive crack models based on the use of non-conventional finite element formulations. Then, some of the existing alternative schemes used to account for the transition from continuum to discrete approaches [8,44,28] will be studied, implemented, tested and compared.

The other developments expected for the near future have as main goal to make even more competitive the HMS and the HD non-conventional formulations described in this paper. Among several research lines, one can mention the following:

(1) to implement p-refinement procedures based on the use of local functions, such as wavelets or Heaviside functions [42]. Using the critical damage concept [13], this refinement may be adaptive;
(2) the non-conventional finite element models allow the use of local refinement functions. This is one important issue when working with damage models, as the non-linear behavior concentrates usually in a specific zone

of the structural domain.

(3) to implement an implicit gradient model in order to avoid the definition of an independent spatial averaging [29–31,15,44]. One of the important advantages of this type of procedure is that the computation of tangent stiffness matrices is simpler than in other types of formulations;
(4) to test the numerical performance of the HMS and HD finite element models when using parallel processing techniques;
(5) to generalise the existing 2D models for 3D analysis;
(6) to generalise the models for cyclic and dynamic analysis.

7 Acknowledgements

This work has been partly supported by "Fundação para a Ciência e Tecnologia" through projects "Financiamento Plurianual", PTDC/ECM/71519/2006 and the PhD scholarship SFRH/BD/9050/2002. The guidance of Professors Claudia Comi and Umberto Perego is gratefully acknowledged.

References

[1] Z.P. Bažant. Instability, ductility, and size effect in strain-softening concrete. *ASCE Journal of Engineering Mechanics*, 102:331–344, 1976.

[2] Z.P. Bažant and M. Jirásek. Nonlocal integral formulations of plasticity and damage: survey of progress. *ASCE Journal of Engineering Mechnics*, 128:1119–1149, 2002.

[3] Z.P. Bažant and G. Pijaudier-Cabot. Measurement of characteristic length of nonlocal continuum. *ASCE Journal of Engineering Mechanics*, 115:755–767, 1989.

[4] M. Cervera, J. Oliver, and R. Faria. Seismic evaluation of concrete dams via continuum damage models. *Earthquake Engineering and Structural Dynamics*, 24:1225–1245, 1995.

[5] C. Cismaşiu. *The hybrid-Trefftz displacement element for static and dynamic structural analysis problems*. PhD thesis, Instituto Superior Técnico, Universidade Técnica de Lisboa, Lisboa, 2000.

[6] C. Comi. Computational modelling of gradient-enhanced damage in quasi-brittle materials. *Mechanics of Cohesive-frictional Materials*, 4:17–36, 1999.

[7] C. Comi. A non-local model with tension and compression damage mechanics. *European Journal of Mechanics A/Solids*, 20:1–22, 2001.

[8] C. Comi, S. Mariani, and U. Perego. From localized damage to discrete cohesive crack propagation in nonlocal continua. In H.A. Mang, F.G. Rammerstorfer, and J. Eberhardsteiner, editors, *Fifth World Congress on Computational Mechanics*, 2002.

[9] C. Comi and U. Perego. A bi-dissapative damage model for concrete with applications to dam engineering. In *ECCOMAS 2000*, 2000.

[10] C. Comi and U. Perego. Fracture energy based bi-dissipative damage model for concrete. *International Journal of Solids and Structures*, 38:6427–6454, 2001.

[11] C. Comi and U. Perego. Nonlocal aspects of nonlocal damage analyses of concrete strucutres. *European Journal of Finite Elements*, 10:227–242, 2001.

[12] C. Comi and U. Perego. Symmetric and non-symmetric non-local damage formulations: an assessment of merits. In *ECCM-2001*, 2001.

[13] C. Comi and U. Perego. Criteria for mesh refinement in nonlocal damage finite element analyses. *European Journal of Mechanics A/Solids*, 23:615–632, 2004.

[14] C. Comi and E. Rizzi. On bifurcation in local and nonlocal materials with tension and compression damage. In *ECCOMAS 2000*, 2000.

[15] R.A.B. Engelen, M.G.D. Geers, and F.P.T. Baaijens. Nonlocal implicit gradient-enhanced elastoplasticity for the modelling of softening behaviour. *International Journal of Pasticity*, 19:403–433, 2003.

[16] J.A.T. Freitas, J.P.M. Almeida, and E.M.B.R. Pereira. Non-conventional formulations for the finite element method. *Computational Mechanics*, 23:488–501, 1999.

[17] J.A.T. Freitas, C. Cismaşiu, and Z.M. Wang. Comparative analysis of hybrid-trefftz stress and displacements elements. *Archives of Computational Mechanics Engineering*, 6:1–26, 1999.

[18] M. Frémond and B. Nedjar. Damage, gradient of damage and principal of virtual power. *International Journal of Solids and Structures*, 33:1083–1103, 1996.

[19] M. Hassanzadeh. *Behaviour of fracture process zone in concrete influenced by simultaneous applied normal and shear displacements*. PhD thesis, Lund Institute of Technology, Lund, 1991.

[20] ICOLD. V international benchmarkworkshop on numerical analysis of dams, theme a2. Denver, Colorado, 1999.

[21] M. Jirásek. Modelling of localized damage and fracture in quasibrittle materials. In P.A. Vermeer et al., editor, *Continuous and discontinuous modelling of cohesive frictional materials, Lecture Notes in Physics 568*, pages 17–29. Springer, Berlin, 2001.

[22] M. Jirásek. *Modeling of localized inelastic deformation, Lecture notes*. Czech Technical University, 2004.

[23] C. LaBorderie. *Phenomenes unilateraux dans un materiau endommageable: modelisation et application a l'analyse de structures en beton*. PhD thesis, Université Paris 6, Paris, 1991.

[24] J. Lee and G. L. Fenves. A plastic-damage concrete model for earthquake analysis of dams. *Earthquake Engineering and Structural Dynamics*, 27:937–956, 1998.

[25] J. Lemaitre. *A course on damage mechanics*. Springer-Verlag, first edition, 1992.

[26] J. Mazars. *Application de la mécanique de l'endommagement au comportement non lineaire et à la rupture du béton de structure*. PhD thesis, Université Paris 6, Paris, 1984.

[27] J. Mazars and G. Pijaudier-Cabot. Continuum damage theory - application to concrete. *ASCE Journal of Engineering Mechanics*, 115:345–365, 1989.

[28] J. Oliver and A.E. Huespe. Continuum approach to material failure in strong discontinuity settings. *Computer Methods in Applied Mechanics and Engineering*, 193:3195–3220, 2004.

[29] R.H.J. Peerlings, R. de Borst, W.A.M. Brekelmans, and J.H.P. de Vree. Gradient-enhanced damage for quasi-brittle materials. *International Journal for Numerical Methods in Engineering*, 39:3391–3403, 1996.

[30] R.H.J. Peerlings, R. de Borst, W.A.M. Brekelmans, J.H.P. de Vree, and I. Spee. Some observations on localization in non-local and gradient damage models. *European Journal of Mechanics A/Solids*, 15(6):937–953, 1996.

[31] R.H.J. Peerlings, M.G.D. Geers, R. de Borst, and W.A.M. Brekelmans. A critical comparison of nonlocal and gradient-enhanced softening continua. *International Journal of Solids and Structures*, 38:7723–7746, 2001.

[32] E.M.B.R. Pereira and J.A.T. Freitas. Numerical implementation of a hybrid-mixed finite element model for reissner-mindlin plates. *Computers & Structures*, 74:323–334, 2000.

[33] G. Pijaudier-Cabot and Z.P. Bažant. Nonlocal damage theory. *ASCE Journal of Engineering Mechanics*, 113:1512–1533, 1987.

[34] C. M. Silva and L. M. S. S. Castro. Hybrid-mixed stress model for the non-linear analysis of concrete structures. In B. H. V. Topping, editor, *The Ninth International Conference on Civil and Structural Engineering Computing*. Civil-Comp Press, 2003.

[35] C. M. Silva and L. M. S. S. Castro. Hybrid-mixed stress formulation with continuum damage models. In P. R. M. Lyra, S. M. B. A. da Silva, F. S. Magnani, and *et al*, editors, *XXV CILAMCE*. Gráfica Bagaço, 2004.

[36] C. M. Silva and L. M. S. S. Castro. Non-conventional finite element models using continuum damage mechanics. In B. H. V. Topping and C. A. Mota Soares, editors, *The Seventh International Conference on Computational Structures Technology*. Civil-Comp Press, 2004.

[37] C. M. Silva and L. M. S. S. Castro. Hybrid and mixed finite element formulations for softening materials. In C. Mota Soares et al., editor, *ECCM-2006*. APMTAC, 2006.

[38] C.M. Silva. *Modelos de Dano em Elementos Finitos Híbridos e Mistos*. PhD thesis, Instituto Superior Técnico, Universidade Técnica de Lisboa, Lisboa, 2006.

[39] C.M. Silva and L.M.S.S. Castro. Hybrid-mixed stress model for the nonlinear analysis of concrete structures. *Computers & Structures*, 83:2381–2394, 2005.

[40] C.M. Silva and L.M.S.S. Castro. Hybrid-mixed stress formulation using continuum damage models. *Communications in Numerical Methods in Engineering*, 22:605–617, 2006.

[41] C.M. Silva and L.M.S.S. Castro. Hybrid-displacement (trefftz) formulation for softening materials. *Computers & Structures*, 85:1331–1342, 2007.

[42] C.M. Silva and L.M.S.S. Castro. Nonlocal damage theory in hybrid-displacement formulations. *International Journal of Solids and Structures*, submitted.

[43] J.C. Simo and J.W. Ju. Strain- and stress-based continuum damage models - i. formulation. *International Journal of Solids and Structures*, 23:821–840, 1987.

[44] A. Simone. *Continuous-discontinuous modelling of failure*. PhD thesis, Delft Technical University, Delft, 2003.

[45] Z. Wang. *Elastoplastic structural analysis with hybrid stress elements*. PhD thesis, Instituto Superior Técnico, Universidade Técnica de Lisboa, Lisboa, 2000.

List of Figures

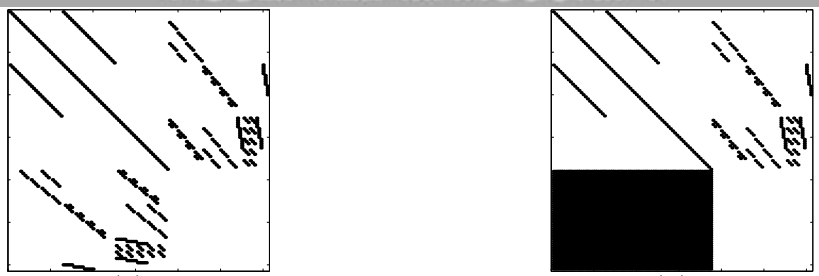

(a) (b)

Fig. 1. Nonzero coefficients in the governing system of one finite element (Equation (10)) (a) without damage and (b) with damage.

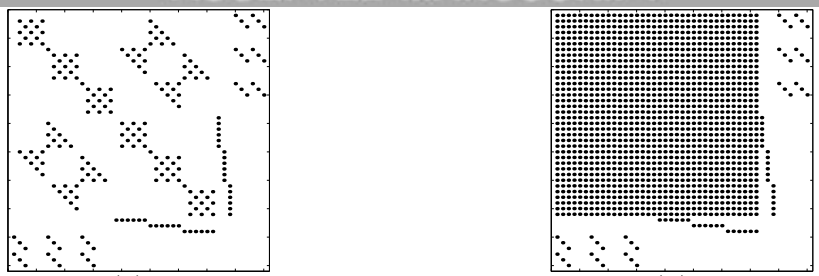

(a) (b)

Fig. 2. Nonzero coefficients in the governing system of one finite element (Equation (16)) (a) without damage and (b) with damage.

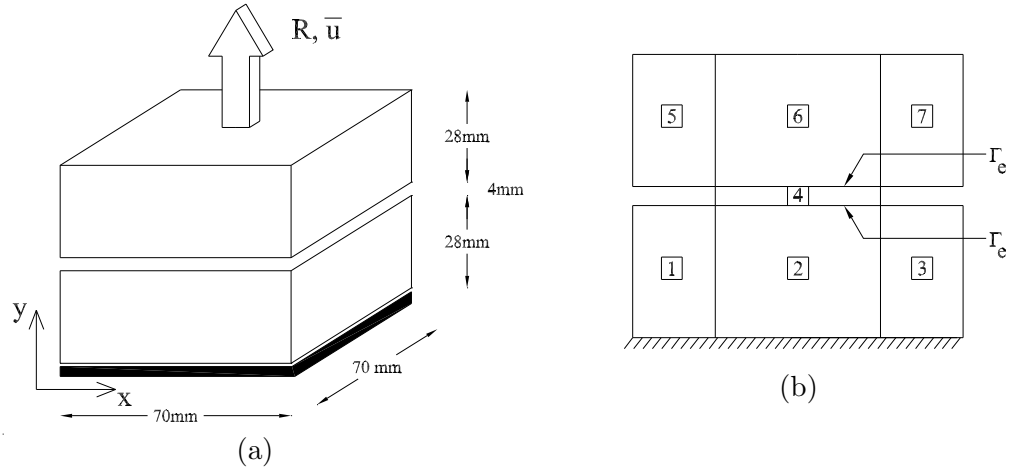

Fig. 3. Hassanzadeh's test [19]: (a) geometry and (b) adopted finite element mesh.

(a) Mesh A. (b) Mesh B.

Fig. 4. Hassanzadeh's test [19]: finite element meshes used in the analysis with FEM [7].

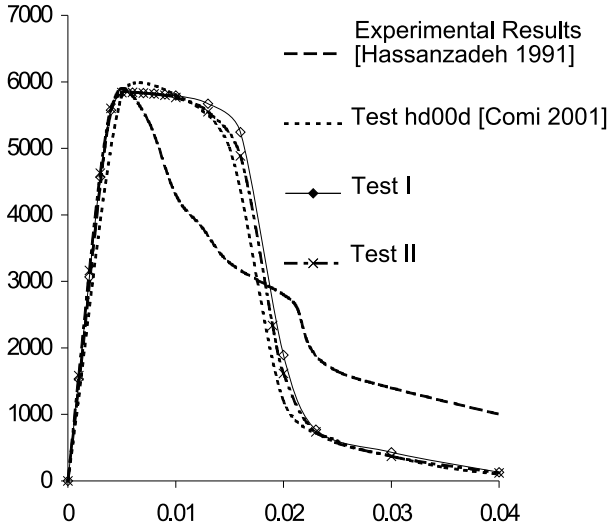

Fig. 5. Hassanzadeh's test [19]: reaction R [N]- prescribed displacement $\overline{u}$ [mm].

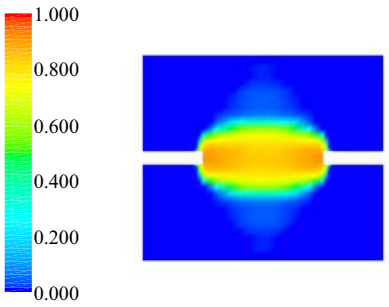

(a) Test I for $\overline{u} = 0.010$ mm.

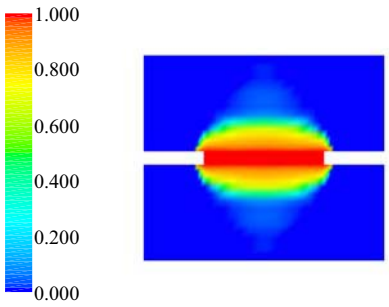

(b) Test I for $\overline{u} = 0.040$ mm.

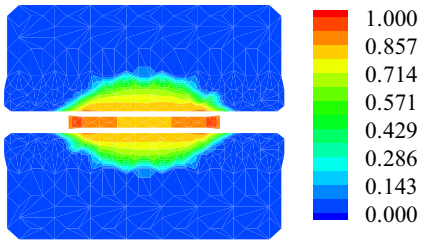

(c) Test hd00d for $\overline{u} = 0.010$ mm [7].

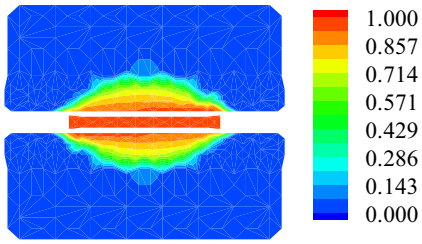

(d) Test hd00d for $\overline{u} = 0.040$ mm [7].

Fig. 6. Hassanzadeh's test [19]: damage [–] distribution evolution obtained with HMS and FEM models.

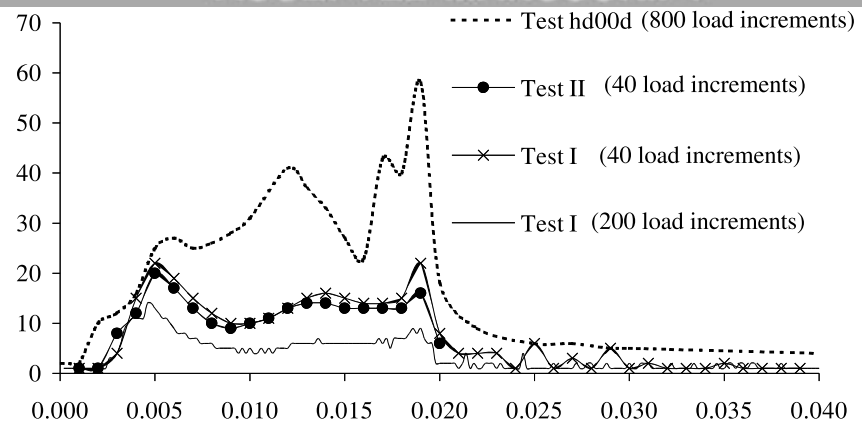

Fig. 7. Hassanzadeh's test [19]: number of iterations versus prescribed displacement $\overline{u}$ [mm] in both HMS and FEM formulations.

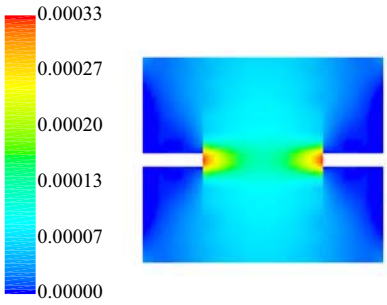

(a) $\overline{u} = 0.005$ mm.

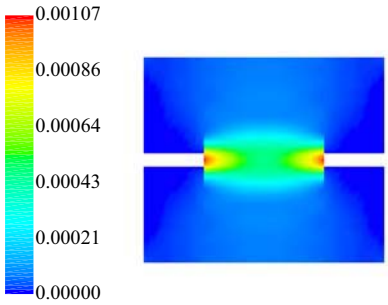

(b) $\overline{u} = 0.010$ mm.

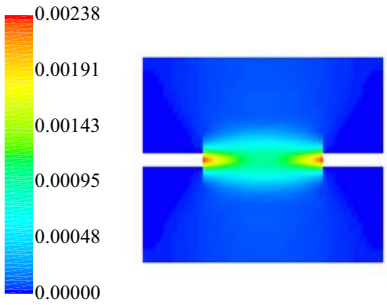

(c) $\overline{u} = 0.015$ mm.

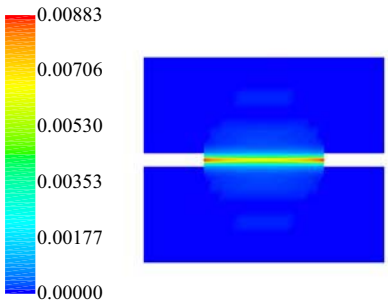

(d) $\overline{u} = 0.020$ mm.

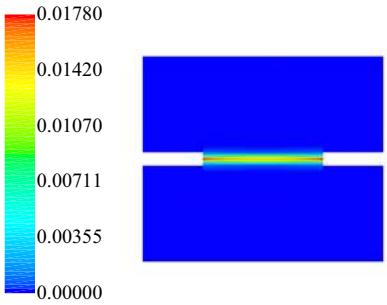

(e) $\overline{u} = 0.030$ mm.

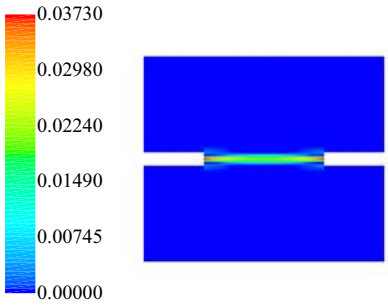

(f) $\overline{u} = 0.040$ mm.

Fig. 8. Hassanzadeh's test [19]: ε_{yy} [–] evolution in Test I.

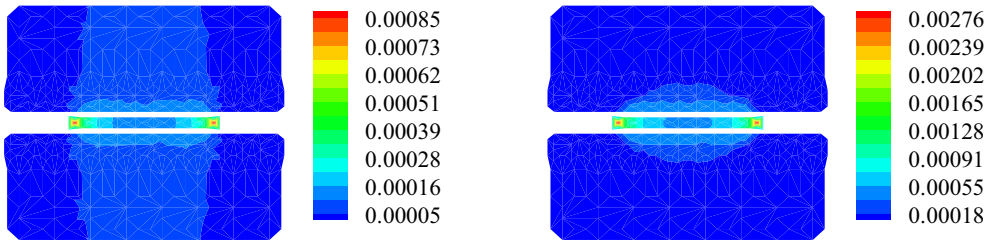

(a) $\overline{u} = 0.005$ mm. (b) $\overline{u} = 0.010$ mm.

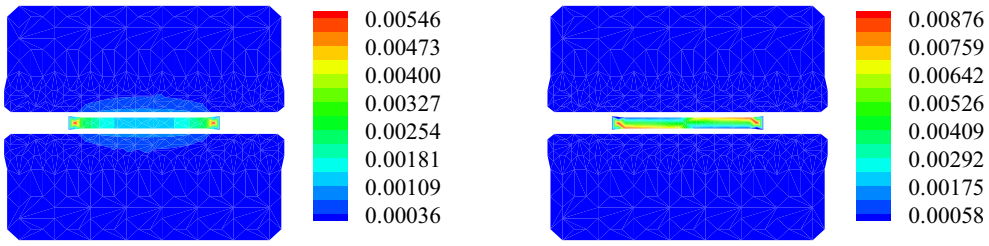

(c) $\overline{u} = 0.015$ mm. (d) $\overline{u} = 0.020$ mm.

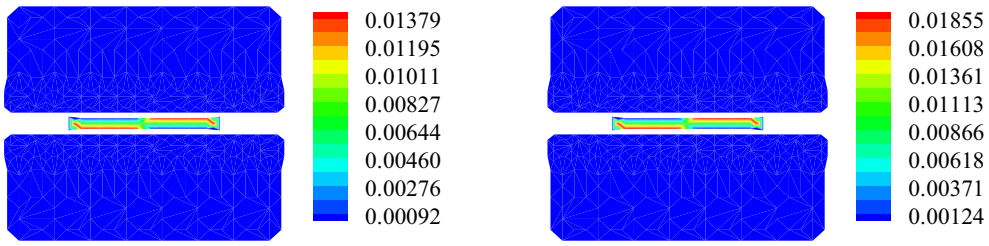

(e) $\overline{u} = 0.030$ mm. (f) $\overline{u} = 0.040$ mm.

Fig. 9. Hassanzadeh's test [19]: ε_{yy} [–] evolution in Test hd00d.

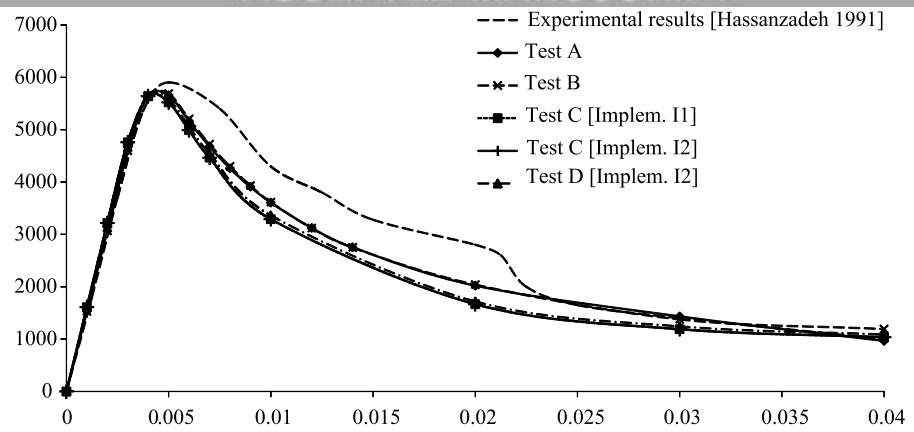

Fig. 10. Hassanzadeh's test [19]: reaction R [N]- prescribed displacement $\overline{u}$ [mm].

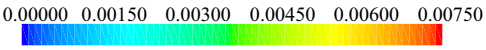

(a) Color scaling

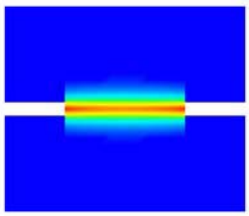

(b) Test A.

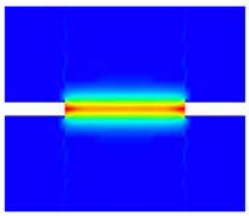

(c) Test B.

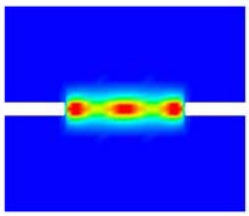

(d) Test C.

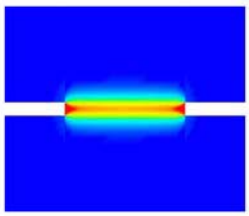

(e) Test D.

Fig. 11. Hassanzadeh's test [19]: ε_{yy} strain field distribution[–] when $\overline{u} = 0.040$ mm.

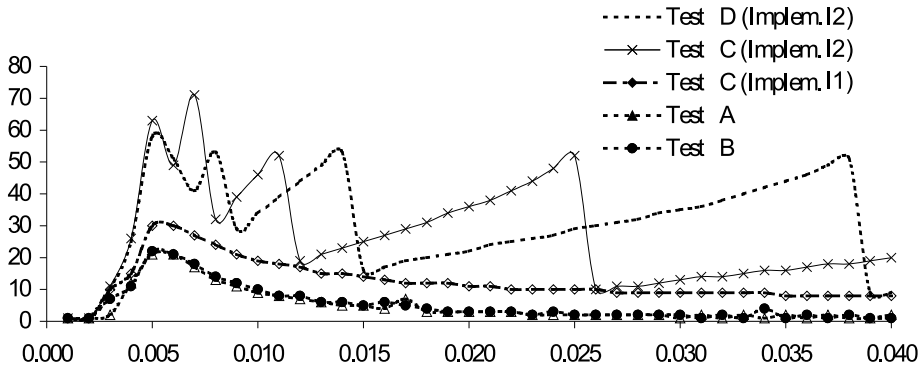

Fig. 12. Hassanzadeh's test [19]: number of iterations versus prescribed displacement $\overline{u}$ [mm] in HMS and HD models.

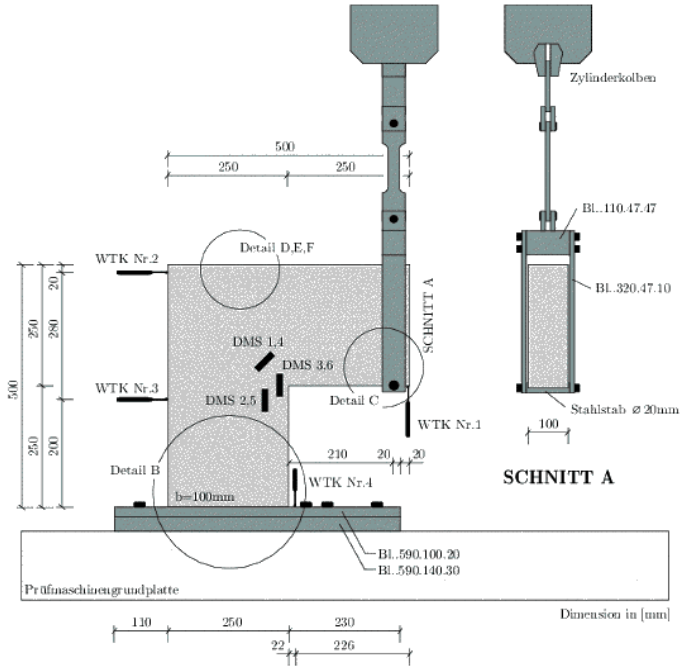

Fig. 13. L-shaped plate: experimental device (available at the NWD-IALAD website)
.

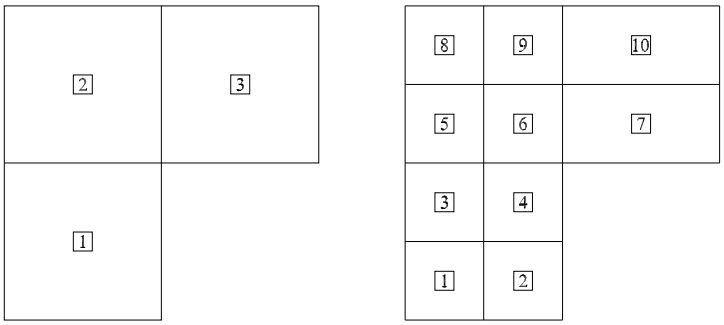

Fig. 14. L-shaped plate: finite element meshes.

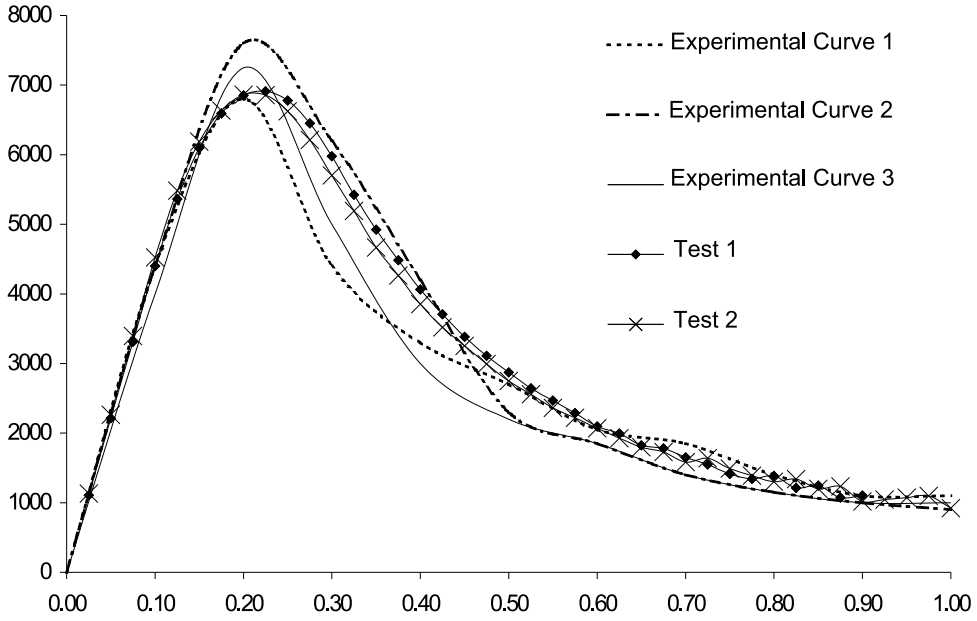

Fig. 15. L-shaped plate: reaction R [N]- prescribed vertical displacement [mm] diagrams.

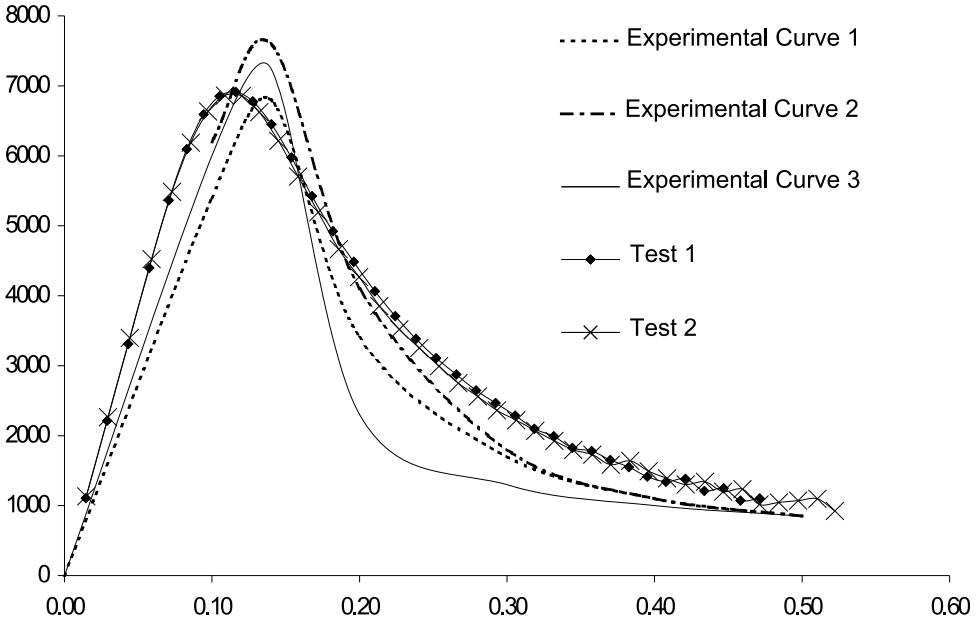

Fig. 16. L-shaped plate: reaction R [N]- horizontal displacement at the upper left corner of the structure [mm] diagrams.

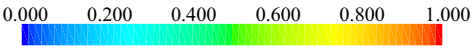

(a) Color scaling.

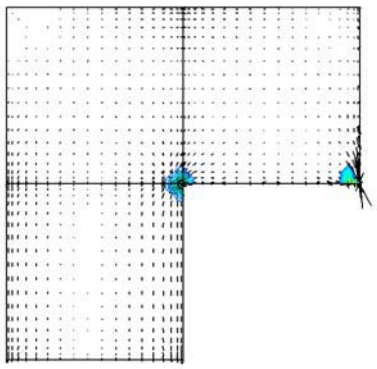

(b) $\overline{u} = 0.125$ mm.

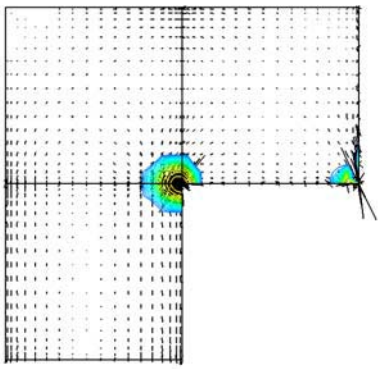

(c) $\overline{u} = 0.175$ mm.

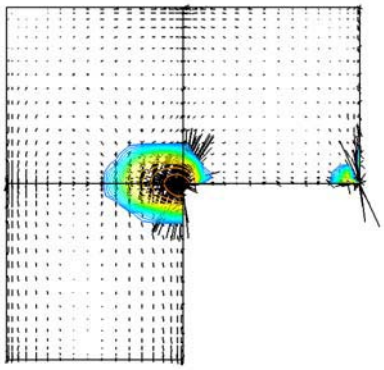

(d) $\overline{u} = 0.250$ mm.

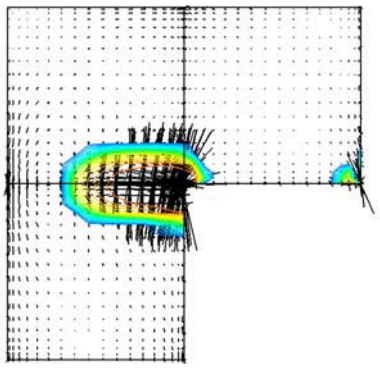

(e) $\overline{u} = 0.375$ mm.

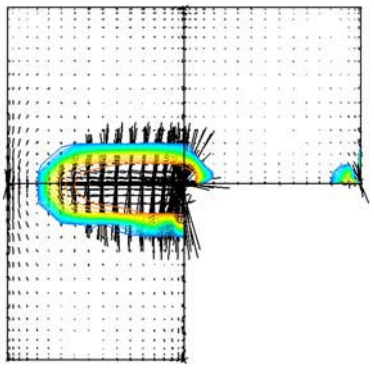

(f) $\overline{u} = 0.500$ mm.

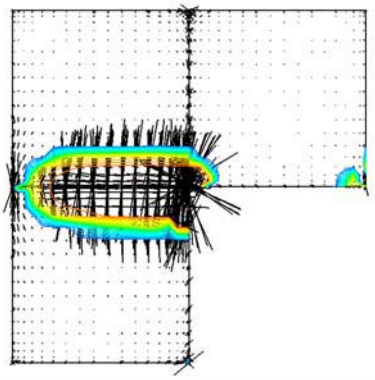

(g) $\overline{u} = 0.750$ mm.

Fig. 17. L-shaped plate, Test 1: damage variable evolution [–] and effective stress tensor principal directions.

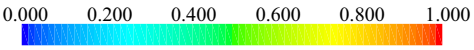

(a) Color scaling.

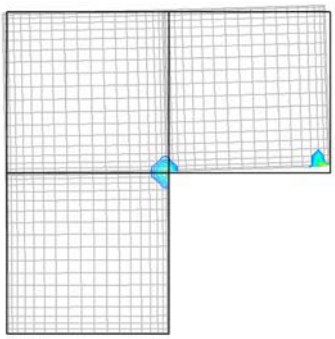

(b) $\overline{u} = 0.125$ mm.

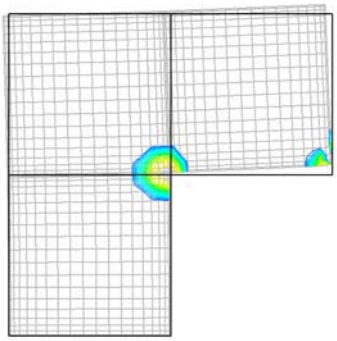

(c) $\overline{u} = 0.175$ mm.

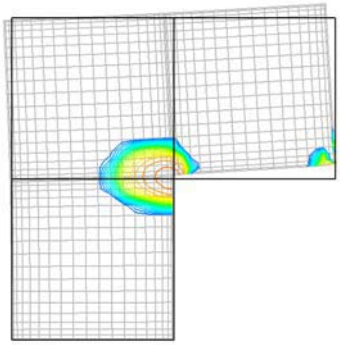

(d) $\overline{u} = 0.250$ mm.

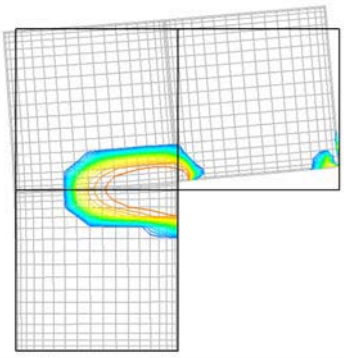

(e) $\overline{u} = 0.375$ mm.

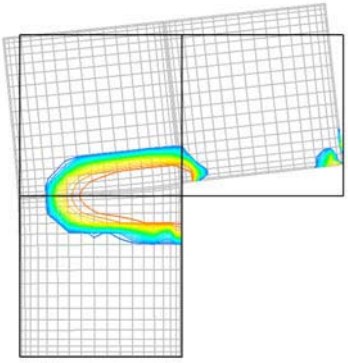

(f) $\overline{u} = 0.500$ mm.

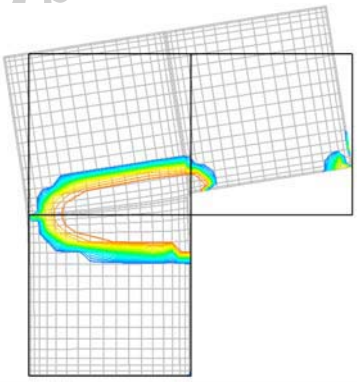

(g) $\overline{u} = 0.750$ mm.

Fig. 18. L-shaped plate, Test 1: damage variable evolution [–] on the structure deformed configuration.

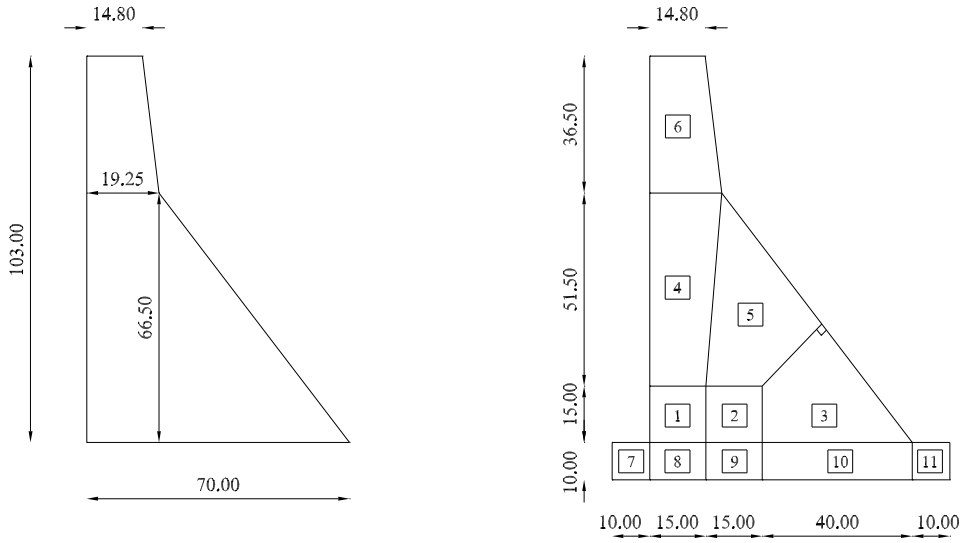

(a) (b)

Fig. 19. Koyna dam: (a) geometry of the structure (dimensions in m) and (b) finite element mesh.

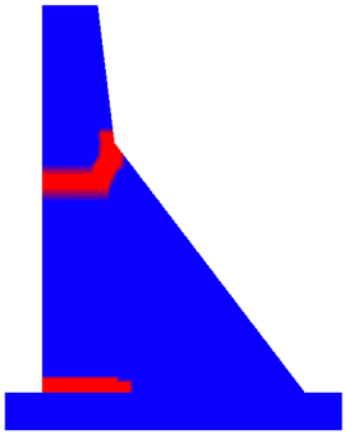

Fig. 20. Koyna dam: qualitative initial damage distribution.

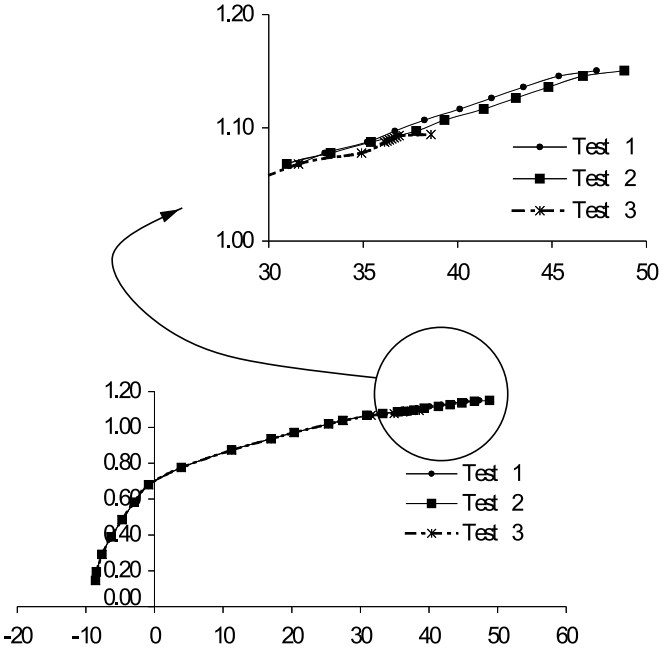

Fig. 21. Koyna dam: evolution of the horizontal curves $q = h_{\text{water}}/h_{\text{dam}}$ - displacement measured at the top of the dam [mm].

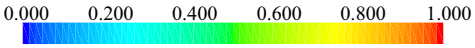

(a) Color scaling.

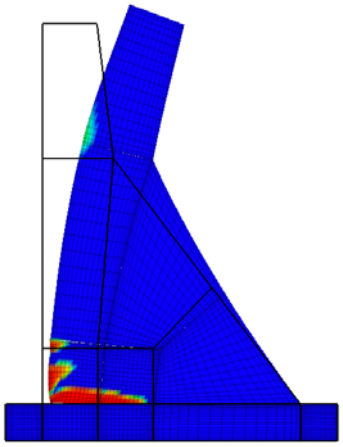

(b) Dam without initial damage.

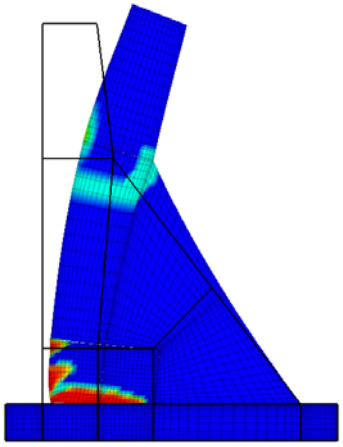

(c) Initial damage of 0.30.

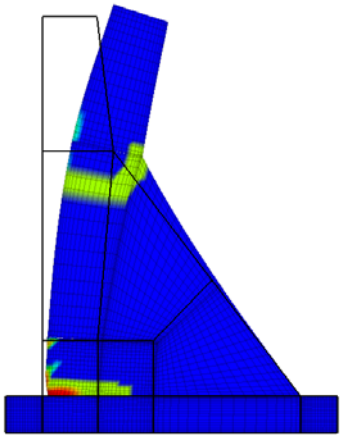

(d) Initial damage of 0.60.

Fig. 22. Koyna dam: damage distribution on the deformed configuration at the final stage of the loading procedure.

List of Tables

Model 1 [25,11,12]	
Damage Variable	d
Helmholtz free energy density[(a)]	$\Psi = \frac{1}{2}(1-d)\,\boldsymbol{\varepsilon}^t\,\mathbf{E}\,\boldsymbol{\varepsilon} + \Psi_{in}(\xi)$ with $\Psi_{in}(\xi) = k\,(1-\xi)\,\sum_{i=0}^{n}\,\frac{n!}{i!}\,\ln^i\left(\frac{c}{1-\xi}\right)$
State equations[(b)]	$\boldsymbol{\sigma} = \frac{\partial \Psi}{\partial \boldsymbol{\varepsilon}} = (1-d)\,\mathbf{E}\,\boldsymbol{\varepsilon}$ $\chi = -\frac{\partial \Psi}{\partial \xi} = -\Psi'_{in}(\xi)$ $Y = -\frac{\partial \Psi}{\partial d} = \frac{1}{2}\,\boldsymbol{\varepsilon}^t\,\mathbf{E}\,\boldsymbol{\varepsilon}$
Activation function	$f(Y-\chi) = Y - \chi = \frac{1}{2}\,\boldsymbol{\varepsilon}^t\,\mathbf{E}\,\boldsymbol{\varepsilon} - \chi$
Evolution laws [(c)]	$\dot{d} = \frac{\partial f}{\partial Y}\,\dot{\gamma} = \dot{\gamma}$ $\dot{\xi} = -\frac{\partial f}{\partial \chi}\,\dot{\gamma} = \dot{\gamma}$
Kuhn Tucker Conditions	$f \leq 0, \quad \dot{d} \geq 0, \quad \dot{d}\,f = 0$
Non-local Variable	$Y = \frac{1}{2}\,\boldsymbol{\varepsilon}^t\,\mathbf{E}\,\boldsymbol{\varepsilon}$

(a) ξ is a scalar internal variable of kinematic nature and variables k, n and c are material parameters.

(b) $\boldsymbol{\varepsilon}$, ξ and d are the state variables and $\boldsymbol{\sigma}$, χ and Y represent the corresponding associated variables.

(c) for this particular damage model, the internal variable ξ coincides with the damage variable d.

Table 1
Continuum damage model with one scalar variable.

Model 2 [9,10,7]	
Damage Variable	$d_t,\, d_c$
Helmholtz free energy density$^{(a,b)}$	$\psi = \frac{1}{2}\left\{2\mu\,\mathbf{e}:\mathbf{e} + k_+\,(tr^+\boldsymbol{\varepsilon})^2 + k_-\,(tr^-\boldsymbol{\varepsilon})^2\right\}$ $\mu = \mu_0(1-d_t)(1-d_c)$ $k_+ = k_0\,(1-d_t)$ if $tr\;\boldsymbol{\varepsilon} \geq 0$ $k_- = k_0\,(1-d_c)$ if $tr\;\boldsymbol{\varepsilon} < 0$ $tr^+\boldsymbol{\varepsilon} = \dfrac{tr\boldsymbol{\varepsilon} + \lvert tr\boldsymbol{\varepsilon}\rvert}{2},\; tr^-\boldsymbol{\varepsilon} = \dfrac{tr\boldsymbol{\varepsilon} - \lvert tr\boldsymbol{\varepsilon}\rvert}{2}$
Constitutive Relation	$\boldsymbol{\sigma} = \frac{\partial\psi}{\partial\boldsymbol{\varepsilon}} = 2\mu\,\mathbf{e} + k_+\,(tr^+\boldsymbol{\varepsilon})\,\mathbf{I} + k_-\,(tr^-\boldsymbol{\varepsilon})\,\mathbf{I}$
Activation functions$^{(c,d,e)}$	$f_t = J_2 - a_t\,I_1^2 + b_t\,r_t\,I_1 - k_t\,r_t^2\,(1-\alpha\,d_c)$ $f_c = J_2 + a_c\,I_1^2 + b_c\,r_c\,I_1 - k_c\,r_c^2$ $r_i(d_i) = \begin{cases} 1 - \dfrac{1-(\frac{\sigma_e}{\sigma_o})_i}{d_{oi}^2}\,(d_{oi}-d_i)^2 & \text{se} \quad d_i < d_{oi} \\ \left[1 - \left(\dfrac{d_i - d_{oi}}{1-d_{oi}}\right)^{c_i}\right]^{0.75} & \text{se} \quad d_i \geq d_{oi} \end{cases}$
Kuhn Tucker Conditions	$f_t \leq 0, \quad \dot{d}_t \geq 0, \quad \dot{d}_t\; f_t = 0$ $f_c \leq 0, \quad \dot{d}_c \geq 0, \quad \dot{d}_c\; f_c = 0$
Non-local Variable$^{(f)}$	$tr^+\boldsymbol{\varepsilon},\; tr^-\boldsymbol{\varepsilon},\; J_{\boldsymbol{\varepsilon}}$

(a) μ_0, k_0 represent the initial undamaged shear and bulk moduli, respectively.
(b) $\mathbf{e}$ denotes the deviatoric part of the small strain tensor.
(c) $a_t, b_t, k_t, a_c, b_c, k_c$ and α are non-negative material parameters.
(d) I_1 corresponds to the stress tensor first invariant and $J_2 = \dfrac{1}{2}\,\mathbf{s}:\mathbf{s}$.
(e) d_{oi} represents the damage value at the peak of the uniaxial diagram.
(g) $J_{\boldsymbol{\varepsilon}} = \dfrac{1}{2}\,\mathbf{e}:\mathbf{e}$.

Table 2
Continuum damage model with two variables.

Model

HMS	Test	I	II
	Mesh (see Figure 3(b))	Mesh 1 (7 elem.)	Mesh 1 (7 elem.)
	$\mathbf{S}_v^\xi$	4	8 (elem. 2, 4, 6) and 5 (others)
	$\mathbf{U}_v^\xi$	3	7 (elem. 2, 4, 6) and 4 (others)
	$\mathbf{S}_v^\eta$	8 (elem. 2, 4, 6) and 4 (others)	8 (elem. 2, 4, 6) and 5 (others)
	$\mathbf{U}_v^\eta$	7 (elem. 2, 4, 6) and 3 (others)	7 (elem. 2, 4, 6) and 4 (others)
	$\mathbf{U}_\gamma^{\xi,\eta}$	3	6 (on $\Gamma_e^{(a)}$) and 3 (others)
	N_{dof}	1153	1885
FEM	Test$^{(b)}$	hd00d	hb00d
	Mesh (see Figure 4)	Mesh A (472 elem.)	Mesh B (908 elem.)
	N_{dof}	492	938

(a) As indicated in Figure 3(b).
(b) Notation adopted by Claudia Comi.
Table 3
Hassanzadeh's test [19]: comparative study of HMS and FEM models.

Formulation

HMS	Test	A	B
	Description	$\mathbf{S}_v^{\xi} = 4$, $\mathbf{U}_v^{\xi} = 3$, $\mathbf{U}_{\gamma}^{\xi,\eta} = 3$ $\mathbf{S}_v^{\eta} = 8$ (elem. 2, 4, 6) and 4 (others) $\mathbf{U}_v^{\eta} = 7$ (elem. 2, 4, 6) and 3 (others)	$\mathbf{S}_v^{\xi,\eta} = 10$, $\mathbf{U}_v^{\xi,\eta} = 9$ $\mathbf{U}_{\gamma}^{\xi,\eta} = 8$
	N_{dof}	1153	4229
	CPU$^{(c)}$ [seconds]	4327	125471

HD	Test	C	D
	Description	$\mathbf{U}_v^{\xi} = 6$ $\mathbf{U}_v^{\eta} = 9$ (elem. 2, 4, 6) 6 (others) $\mathbf{T}^{\xi,\eta} = 5$	$\mathbf{U}_v^{\xi} = 9$ (elem. 2, 4, 6) 4 (others) $\mathbf{U}_v^{\eta} = 9$ (elem. 2, 4, 6) 4 (others) $\mathbf{T}^{\xi,\eta} = 3$ except $\mathbf{T}^{\eta}_{\text{elem 4}} = 8$
	N_{dof}	956	906
	CPU$^{(c)}$ [seconds]	6824 (I2)$^{(a)}$ and 152755 (I1)$^{(b)}$	9586 (I2)$^{(a)}$

(a) As explained in Section 4 and adopting the value 50 as the maximum number of iterations at the previous load step.
(b) As defined in Section 4.
(c) In a Pentium 4 machine, 2996 Mhz.

Table 4
Hassanzadeh's test [19]: comparative study of HMS and HD models.